

RESEARCH ARTICLE

Coordination of carbon fixation and nitrogen metabolism in *Salicornia europaea* under salinity: Comparative proteomic analysis on chloroplast proteins

Pengxiang Fan, Juanjuan Feng, Ping Jiang, Xianyang Chen, Hexigeduleng Bao, Lingling Nie, Dan Jiang, Sulian Lv, Tingyun Kuang and Yinxin Li

Key Laboratory of Plant Molecular Physiology, Institute of Botany, Chinese Academy of Sciences, Beijing, P. R. China

Halophyte, like *Salicornia europaea*, could make full use of marginal saline land for carbon fixation. How the photosynthesis of *S. europaea* is regulated under high salinity implicates a significant aspect to exploit this pioneer plant in future. Measurement of photosynthesis parameters demonstrated the reduction of photosynthesis for the 0 and 800 mM NaCl treated plants are more likely due to non-stomatal limitation, which might be caused by changes in the enzymes associated with photosynthesis. Different salinity induced ultrastructure changes other than photosynthetic apparatus damage, suggesting the photosynthesis of *S. europaea* might be affected via biochemical regulation. Comparative proteomics analysis of chloroplast proteins by 2-D gel electrophoresis reproducibly detected 90 differentially expressed proteins, among which 66 proteins were identified by nanoLC MS/MS. Further study of thylakoid membrane proteins by Blue-Native PAGE proved the increase in abundance of light reaction proteins under salinity. Analysis of gene expression patterns of 12 selected proteins provides evidence for the correlations between transcription and proteomics data. Based on our results, a putative model of photosynthesis regulatory network figured out proper coordination of carbon fixation and nitrogen metabolism in chloroplast of *S. europaea* under salinity, which provided subcellular level insight into salt tolerance mechanism in *S. europaea*.

Received: January 27, 2011

Revised: August 16, 2011

Accepted: August 18, 2011

**Keywords:**

Carbon fixation / Chloroplast proteomics / Halophyte / Nitrogen metabolism / Photosynthesis / Plant proteomics

1 Introduction

Saline land contains high level of salt as well as very low quantity of nutrition elements, which severely constrains agricultural plant worldwide [1–3]. High concentration of soil salts often causes ion imbalance, hyperosmotic stress,

nutrient deficiency in plants [4–8], and eventually inhibited the growth of plants. The decline in growth for lots of plants under salt stress is usually accompanied by the reduction of photosynthetic activity [9, 10]. After the onset of salt stress, the inhibition of photosynthesis is mainly caused by temporary decreased stomatal conductance [10, 11]. After

Correspondence: Professor Yinxin Li, Key Laboratory of Plant Molecular Physiology, Institute of Botany, Chinese Academy of Sciences, No. 20 Nanxincun, Xiangshan, Haidian District, Beijing 100093, P. R. China

E-mail: yxli@ibcas.ac.cn

Fax: +86-10-82596139

Abbreviations: **BN**, Blue-Native; **C_i**, intercellular CO₂ concentration; **Cond**, stomatal conductance for water vapor; **DM**, *n*-dodecyl β-D-maltoside; **DW**, dry weight; **EF-Tu**, elongation factor Tu; **FBP**, fructose-bisphosphate; **FW**, fresh weight;

NPQ, non-photochemical quenching; **OPP**, oxidative pentose-phosphate pathway; **P_n**, net photosynthetic rate; **PRK**, phosphoribulokinase; **PS**, photosystem; **qRT-PCR**, quantitative RT-PCR; **RbcL**, Ribulose-1,5-bisphosphate carboxylase/oxygenase large subunit; **RCA**, RuBisCO activase; **RuBisCO**, Ribulose-1,5-bisphosphate carboxylase/oxygenase; **RWC**, relative water content; **SOD**, superoxide dismutase; **TK**, transketolase; **Tr**, transpiration speed; **6PGDH**, plastidic 6-phosphogluconate dehydrogenase

Colour Online: See the article online to view Figs. 1, 4, 5 in colour.

long duration, the Na^+ accumulation in leaves may decrease the stability of photosystem II (PSII) functions and inhibit photosynthetic electron transport [9, 10, 12–18]. Then, the structural alterations and functional loss in thylakoid membranes may damage the photosynthetic apparatus, and eventually reduce the carbon assimilation rate [14, 19]. However, many halophytes capable of tolerating a wide range of salinity could maintain normal or even increased photosynthesis activity on the saline soil, with carbon fixation unaffected or even stimulated [15, 20, 21]. Understanding on how these plants maintain high photosynthesis capacity and sustain growth under salinity is meaningful for the efficient utilization of halophytes on marginal saline land. Several attempts had been made to elucidate the mechanism of photosynthesis of halophyte under salinity, by working on the photosynthesis performance at a whole plant level [15, 22, 23] or focusing on particular chloroplast enzymes that might contribute to high salinity tolerance in halophytes [24, 25], while few works have been reported to identify the photosynthetic network under salinity in halophytes at a subcellular level. The subcellular proteomic analysis has been proved to be a powerful method for refining the knowledge of cellular process network in one particular organelle [26]. With the use of proteomics approach, many studies have been focused on the protein changing patterns in the organelles of plants in response to environment stress, including mitochondria [27], nuclear [28], or plasma membranes [29]. A new research also focused on investigating the proteome dynamics of rice plastid in the de-etiolation process [30]. Recently, a study was carried out to investigate the effects of salinity on the proteome of maize chloroplasts in the initial phase of salt stress [31]. Many researches on halophytes have applied proteomics approaches, which represents an important source for unraveling salt tolerance mechanisms and identifying new targets for plant improvement [32–35]. However, no research has been performed to analyze the chloroplast proteome of halophytes, which might possess unique regulatory mechanism of photosynthesis under salinity.

As a succulent halophyte belonging to Chenopodiaceae, *Salicornia europaea* is considered to be one of the most salt-tolerant plant species in the world [36, 37]. Some economic advantageous aspects of this plant exist in their application on marginal saline land as an edible vegetable and oilseed crop or as a promising candidate to be included in life support systems in space stations [38, 39]. Meanwhile, this species is also considered as a good research material to study high salt tolerance mechanism in plant [40]. Previous researches have proved that *S. europaea* is a C_3 plant [41–43], which has no special anatomical structure to facilitate carbon assimilation as in the C_4 or Crassulacean acid metabolism plant, indicating that chloroplast is the key site where the regulatory photosynthesis events of this plant takes place under salinity.

In the present study, we initiated the subcellular proteomic investigation of chloroplast proteins in *S. europaea*. By the application of 2-DE and Blue-Native (BN) PAGE in combination with MS/MS analysis, we characterized

proteins whose expressions were altered under salt treatment. Identification of these differentially expressed proteins as well as the investigation for impacts of salinity on photosynthesis parameters and chloroplast ultrastructure reveal a close linkage between the specific proteins with changed abundance and the photosynthesis alteration under different salinity. Then, we propose a putative photosynthesis network of *S. europaea* under different salinities.

2 Materials and methods

2.1 Plant materials and growth conditions

S. europaea seeds were collected from coastal area in Dafeng City, Jiangsu Province of China. They were sown on vermiculite irrigated with tap water. After germination, seedlings were grown in a greenhouse with day/night temperature regime $25^\circ\text{C}/20^\circ\text{C}$, photoperiod 16 h, relative humidity $50 \pm 10\%$. Seedlings were irrigated weekly with half-strength Hoagland nutrient solution. After sowing for 40 days, the plants were divided into three groups and were salinized with 200 mM incremental intervals each day to final concentrations of 0, 200, and 800 mM NaCl, respectively. Then, they were irrigated in the morning with a 3-day interval for an additional 30 days before they were harvested for further analysis.

2.2 Plant weight, relative water content, and chlorophyll measurements

Fresh weight (FW) of shoot was determined immediately after plant harvesting. Dry weight (DW) was measured after drying for 48 h in an oven at 80°C . Relative water content (RWC) of plant was calculated as follows: $\text{RWC} = (\text{FW} - \text{DW})/\text{FW} \times 100\%$. For chlorophyll measurement, the FW of young shoots from different treated plants were measured after washing with distilled water; then the tissues were extracted in 80% v/v acetone. Chlorophyll content was determined by the method of Porra et al. [44]. Six replicates were measured for each treatment.

2.3 Photosynthesis parameters measurements

Chlorophyll fluorescence emission was analyzed by a PAM-101 chlorophyll fluorimeter (Walz, Germany) followed the protocol described by Hichem et al. [12]. In brief, measurements were made on each plant in each of the three salinity treatments ($n = 6$). To measure the minimal fluorescence (F_0) and the maximal fluorescence (F_m), the plants were dark-adapted for at least 30 min. Then, the shoots were illuminated with continuous white actinic light with photon density $500 \mu\text{mol}/\text{m}^2/\text{s}$, and the steady-state value of fluorescence (F_s) were recorded. After a series of saturating pulse

at $8000 \mu\text{mol}/\text{m}^2/\text{s}$, the maximal fluorescence value in light-adapted shoots (F_m') were measured. The minimum fluorescence value of light-adapted shoots was determined by $F_o' = F_o / [(F_v/F_m) + (F_o/F_m')]$ [45]. Fluorescence parameters were calculated as described by Maxwell and Johnson [46]. The maximum efficiency of PSII in the dark-adapted state was determined by $F_v/F_m = (F_m - F_o)/F_m$; the efficiency of excitation capture by open PSII centers was calculated as $F_v'/F_m' = (F_m' - F_o')/F_m'$; Nonphotochemical quenching was determined by NPQ (non-photochemical quenching) $= (F_m - F_m')/F_m'$; photochemical quenching was calculated as $q_p = (F_m' - F_s)/(F_m' - F_o')$.

Photosynthetic gas exchange parameters were determined by a gas exchange system (LI-6400, LI-COR, USA), coupled with a LED light source. The net photosynthetic rate (P_n), stomatal conductance for water vapor (Cond), intercellular CO_2 concentration (C_i) and transpiration speed (Tr) were determined at a constant light photon density ($1200 \mu\text{mol}/\text{m}^2/\text{s}$), and an ambient CO_2 concentration of $450 \mu\text{mol}/\text{mol}$. Photosynthetic area was approximated as half the area of the cylindrical branches, as only the upper half received unilateral illumination in the leaf chamber.

2.4 Transmission electron microscopy analysis

For ultrastructural examinations of chloroplasts, samples taken from *S. europaea* shoot were fixed in 2.5% glutaraldehyde in 100 mM phosphate buffer (pH 7.0) for 4 h at room temperature, followed by 2 h of postfixation in 1% OsO_4 , rinsed with phosphate buffer. Then, the samples were dehydrated by graded ethanol solutions and embedded in a low viscosity epoxy resin mixture for polymerization at 60°C for 24 h. The blocks were sectioned with a glass knife using an ultramicrotome and were collected onto copper grids, which were then sequentially stained with uranyl acetate followed by lead citrate and examined under a JEOL JEM-1230 transmission electron microscope.

2.5 Chloroplast proteins extraction and 2-DE

The procedures of chloroplast isolation, chloroplast proteins extraction, and 2-DE were according to our reported method [47]. The washed protein pellets were air-dried and recovered with lysis buffer (7 M urea, 2 M thiourea, 2% CHAPS, 13 mM DTT, 1.7% PMSF, 1% IPG buffer). Protein concentration was determined following the Bradford method [48], using BSA as the standard. The calibration curve was determined using BSA solution with a concentration from 1.0 to 10.0 mg/mL.

The sample containing 900 μg of total proteins was loaded onto an IPG strip holder with 24 cm, pH 4–7, linear gradient IPG strips (GE Healthcare, Uppsala, Sweden), and rehydrated for 24 h at room temperature. Then, focusing was performed on the IPGphor apparatus under the

following conditions: 100 V for 2 h, 300 V for 1 h, 500 V for 1 h, 1000 V for 1 h, a gradient to 8000 V for 2 h, and 8000 V up to 80 000 Vh. After IEF, these strips were equilibrated with equilibration solution (50 mM Tris, pH 8.8, 6 M urea, 30% glycerol, 2% SDS, 0.002% bromophenol blue) containing 1% DTT for 15 min, and subsequently with equilibration solution containing 4% iodoacetamide for another 15 min. The second dimension proteins separation was performed on an Ettan DALT System: 7 W for 45 min and 18 W for 6 h for every strip at a constant temperature of 16°C .

2.6 Gel staining, imaging, and data analysis

The 2-D gels were visualized according to the modified CBB staining method [49]. The stained gels were scanned by UMAX Power Look 2100XL scanner (UMAX, Taipei, China) at 600 dpi (dots per inch) resolutions, and image analysis was performed with Image Master 2D Platinum Software (Version 5.0, GE Healthcare) following the user's manual. To account for experimental variation, three biological replicate gels resulting from three independent experiments were analyzed for chloroplast proteins extracted from 0, 200, and 800 mM NaCl treated plants. Each spot volume value was divided by the sum of total spot volume values to obtain individual relative volumes of the detected spots. The normalized intensity of spots on three replicate 2-D gels was averaged and one-way ANOVA test was used to determine whether the relative change was statistically significant between samples using SPSS software (SPSS, Chicago, IL). Experimental M_r (kDa) of each protein was estimated by comparison with the M_r markers, and experimental pI was determined by its migration on the IPG. Only those spots that reproducibly changed in abundance more than 1.5-fold and passed the test ($p \leq 0.05$) were considered to be differentially expressed proteins and selected for protein identification.

2.7 Protein identification

The protein was digested in-gel with bovine trypsin (Trypsin, Roche, Cat. No. 11418025001) as described previously [50]. Peptide extracts were vacuum drying. Then, they were resuspended in 20 μL of ultrapure water and ready for MS analysis.

LC MS/MS analysis was performed in a linear ion trap mass spectrometer LTQ (ThermoFinnigan, San Jose, CA) coupled with an HPLC system as described previously [51]. In brief, the peptide extracts were loaded on the HPLC, which was linked to an in-house packed C18 capillary column with 10 cm in length and 100 μm in inner diameter. To reduce dead volume, high voltage of 2.55 kV was applied to the column in the HPLC side through a connector. The peptide extracts were sequentially eluted with a gradient of 0–90% of

buffer B (80% ACN, 0.1% formic acid) in buffer A (5% ACN, 0.1% formic acid) at a flow rate of about 500 nL/min. After spraying from the capillary column to the LTQ instrument, the eluted peptides were applied to MS analysis. The instrument measured the intensity of peptide ions with the mass range of m/z 400–2000, which was performed in a data-dependent mode. The peptide with the highest intensity was isolated and subjected to collision-induced dissociation. The XCalibur data system (ThermoElectron, Waltham, MA, USA) was used to control the HPLC solvent gradients and the application of MS scanning functions. All tandem spectra were submitted to a local MASCOT (Matrix-Science, London, UK) server and searched against the taxonomy of Viridiplantae in the NCBI (NCBI nr) database (as of Mar 2010) with the following criteria. Searches were done with a mass tolerance of 2 Da in MS mode and 0.8 Da in MS/MS mode. One missed cleavage per peptide was allowed and variable modifications were taken into account such as carbamidomethylation of cysteine and oxidation of methionine. The identification was considered only with a higher MASCOT score and additional experimental confirmation of the protein spots on the 2-DE gels.

2.8 Protein classification and hierarchical cluster analysis

The annotations of the identified proteins combined with the result of BLAST alignments provided the biological function of the proteins. The proteins were functionally classified according to the MapMan ontology, (<http://mapman.gabipd.org/>) using classes initially defined by Thimm et al. [52] and Usadel et al. [53] for Arabidopsis genes. Then, these proteins were analyzed by TargetP (<http://www.cbs.dtu.dk/services/TargetP/>) to predict their subcellular location. Hierarchical clustering of the expression profiles was performed on the log transformed fold change expression values for the identified protein spots using GenePattern platform as described previously (<http://www.broadinstitute.org/cancer/software/genepattern/>) [54].

2.9 Western blot analysis

Immunoblot analysis was used to examine the purity of chloroplast proteins with antibodies against proteins from different cell compartments and to determine the Ribulose-1,5-bisphosphate carboxylase/oxygenase (RuBisCO) expression levels in *S. europaea* under different salinity. Equal amount of 4 µg proteins were separated by SDS-PAGE and transferred to PVDF membranes (GE, USA) using a wet transblot system (Bio-Rad, USA). The chloroplast proteins or total proteins were immunoblotted using polyclonal antibody raised against Ribulose-1,5-bisphosphate carboxylase/oxygenase large subunit (RbcL), β -actin, histone proteins H3, plant PsbP, PsbO, and Lhcb2, (Agrisera,

Sweden) and were visualized by alkaline phosphatase using BCIP/NBT as substrate. The immunoblot experiments were repeated at least three times and the representative figures are shown.

2.10 Thylakoid membrane preparation, BN-PAGE, and SDS-PAGE

Thylakoid membranes of *S. europaea* were prepared by a standard method as described previously [55]. BN-PAGE and SDS-PAGE were carried according to the reported methods [56, 57]. In brief, shoots of the plants were homogenized in isolation buffer at 4°C (400 mM sucrose, 50 mM HEPES-KOH, pH 7.8, 10 mM NaCl, and 2 mM $MgCl_2$). The homogenate was filtered with two layers of cheesecloth and the supernatant removed by centrifugation at $5000 \times g$ for 10 min. Then, the thylakoid pellets were rinsed with isolation buffer. After recentrifugation, the pellets were resuspended in isolation buffer and ready for use. Chlorophyll content was determined as described previously [44]. The thylakoid membranes with equal content of chlorophyll were then washed with 330 mM sorbitol, 50 mM BisTris-HCl, pH 7.0. Then, the resuspension buffer containing 20% glycerol and 25 mM BisTris-HCl, pH 7.0 was used to suspend the thylakoid membranes pellets. *n*-dodecyl β -D-maltoside (DM) was added to the thylakoid suspension to reach the final concentration 1% w/v. The suspension was incubated for at least 10 min at 4°C and centrifugation at $12000g$ for 10 min. After that, 5% w/v Serva blue G dissolved in 100 mM BisTris-HCl, pH 7.0, 500 mM 6-amino-*n*-caproic acid, and 30% glycerol was added to the supernatant to reach the final concentration of 0.5% w/v and was ready for use. The samples were separated by 0.75-mm-thick, 5–12% gradient gels in a vertical electrophoresis apparatus with a cooling system (GE Healthcare). After electrophoresis, the gels were scanned and analyzed using an AlphaImager 2200 system. Then, the lanes were excised from the BN-PAGE gels and were immersed in SDS buffer and 5% β -mercaptoethanol for 30 min. After that, the proteins in a single lane were separated in the second dimension by 12.5% SDS polyacrylamide gels with 6 M urea, and dyed with CBB after electrophoresis. Gels of three biological replicates were scanned and analyzed.

2.11 Cloning of partial sequences of select protein-encoding genes

The PCR-based strategy using degenerate primers was undertaken to obtain the partial sequence of selected protein-encoding genes. The sequences of selected identified proteins were searched for homologs by BLASTP (www.ncbi.nlm.nih.gov/BLAST/). The Consensus Degenerate Hybrid Oligonucleotide Primers (CODEHOP)

approach [58] was used to identify conserved amino acid stretches for the selected proteins and to design of degenerate primers anchored to the conserved structural motifs. The partial fragments of target genes were amplified using the degenerate primers from cDNA of *S. europaea* by PCR, and the products were cloned using the TA cloning kit (Transgene, Beijing) and sequenced. The obtained EST sequences were further verified by searching in NCBI with BLASTP, which were then submitted to the Express Sequence Tags Database at NCBI (<http://www.ncbi.nlm.nih.gov/projects/dbEST/>), with the accession numbers listed in Supporting Information Table S3.

2.12 Real-Time quantitative RT-PCR

Total RNA was isolated from young shoot of *S. europaea* as described previously [59] and then treated with RNase-free DNase I. A total of 0.5 µg RNA was used for the first-strand cDNA synthesis with Reverse Transcriptase kit (Transgene, Beijing). Three independent samples for each treatment were used for the quantitative assays, which were performed with an Mx3000P system (Stratagene) by use of the SYBR Green Realtime PCR Master Mix according to the manufacturer's protocol (TOYOBO, Japan). α -Tubulin of *S. europaea* was used as internal control as proposed by Momonoki et al. [60]. Gene-specific primers were designed according to the obtained partial sequence of the genes as listed in Supporting Information Table S3. The relative quantification method ($2^{-\Delta\Delta C_t}$) was used to evaluate quantitative variation between different treatments.

2.13 Statistical analysis

The statistical results are presented as means \pm SD. Statistical analysis were performed by one-way ANOVA and Duncan's multiple range tests with 5% level of significant, using the SPSS software (version 12.0).

3 Results

3.1 Photosynthesis performances

Halophyte maintains optimal growth at moderate salinity, while the growth declines at either non-saline or supra-optimal salinity [20, 21, 24, 33]. In order to explain the growth response to salinity by photosynthetic physiology, we examined the chlorophyll content, chlorophyll fluorescence, and gas-exchange parameters for *S. europaea* plant treated with 0, 200, and 800 mM NaCl for 30 days (Fig. 1A). The 200 mM NaCl-treated plants had both significant higher DW and RWC than the other two treatments (Figs. 1C and D). Young shoots of non-saline treated plants had both chlorophyll *a* and *b* content significantly higher than the salt-

treated ones (Fig. 1E). After that, chlorophyll fluorescence was measured to provide detailed information about PSII as shown in Figs. 1F–I. The results demonstrated that the ratio F_v/F_m , a measure of the maximum quantum yield of photosynthesis, as well as the parameter F_v/F_m' , which provides an estimate to efficiency of excitation energy capture by open PSII reaction centers, were the highest for 200 mM NaCl treatment, while q_p was shown to have a tendency similar to F_v/F_m and F_v/F_m' . The NPQ of chlorophyll fluorescence for non-saline treated plant was observed to be considerably higher than the other two treatments, indicating the growing environment without salt does cause an increase in thermal dissipation in PSII antennae, which often serves as strategy for plant to prevent their photosynthetic capacity from being damaged under stress conditions [45, 46]. Gas exchange parameters were measured under saturating light and atmospheric CO₂, which showed responses to salinity (Figs. 1K–M). P_n was stimulated by salinity treatments up to 200 mM, and underwent a drastic reduction with 800 mM NaCl treatment. The Cond and Tr showed no significant difference for 0 and 200 mM NaCl-treated plants, while both reduced in 800 mM NaCl treatment. In the meantime, a negative correlation was observed between C_i and P_n for all three treatments.

3.2 Chloroplast ultrastructure observation

In order to find whether salinity induces morphological changes in photosynthetic organelle, *S. europaea* plants under different NaCl concentrations were prepared for chloroplast ultrastructure observation (Fig. 1B). Under 0 mM NaCl condition, the chloroplast showed a slim spindle shape with a typical lamellar granal structure consisting of thylakoid, which was slightly dense. In the 200 mM NaCl-treated plants, the chloroplasts were observed to be slightly swollen. In this case, the granal thylakoid inside the chloroplast were expanded, making the lumenal volume of the swelling thylakoid increased. Following the 800 mM NaCl treatment, the chloroplasts showed a globular shape due to severe swelling. However, this high concentration of NaCl treatment did not induce swell of the granal thylakoid; instead, the grana became compact with the volume of thylakoid lumen reduced apparently.

3.3 Chloroplast proteins extraction and purity assessment

Chloroplasts were isolated from *S. europaea* treated with 0, 200, and 800 mM NaCl for 30 days, and the purity of chloroplasts was assessed by measuring the activity of catalase enzyme which is an indirect cytosolic marker in the chloroplast fraction as described in our previous report [47]. In this study, the purity of proteins extracted from the

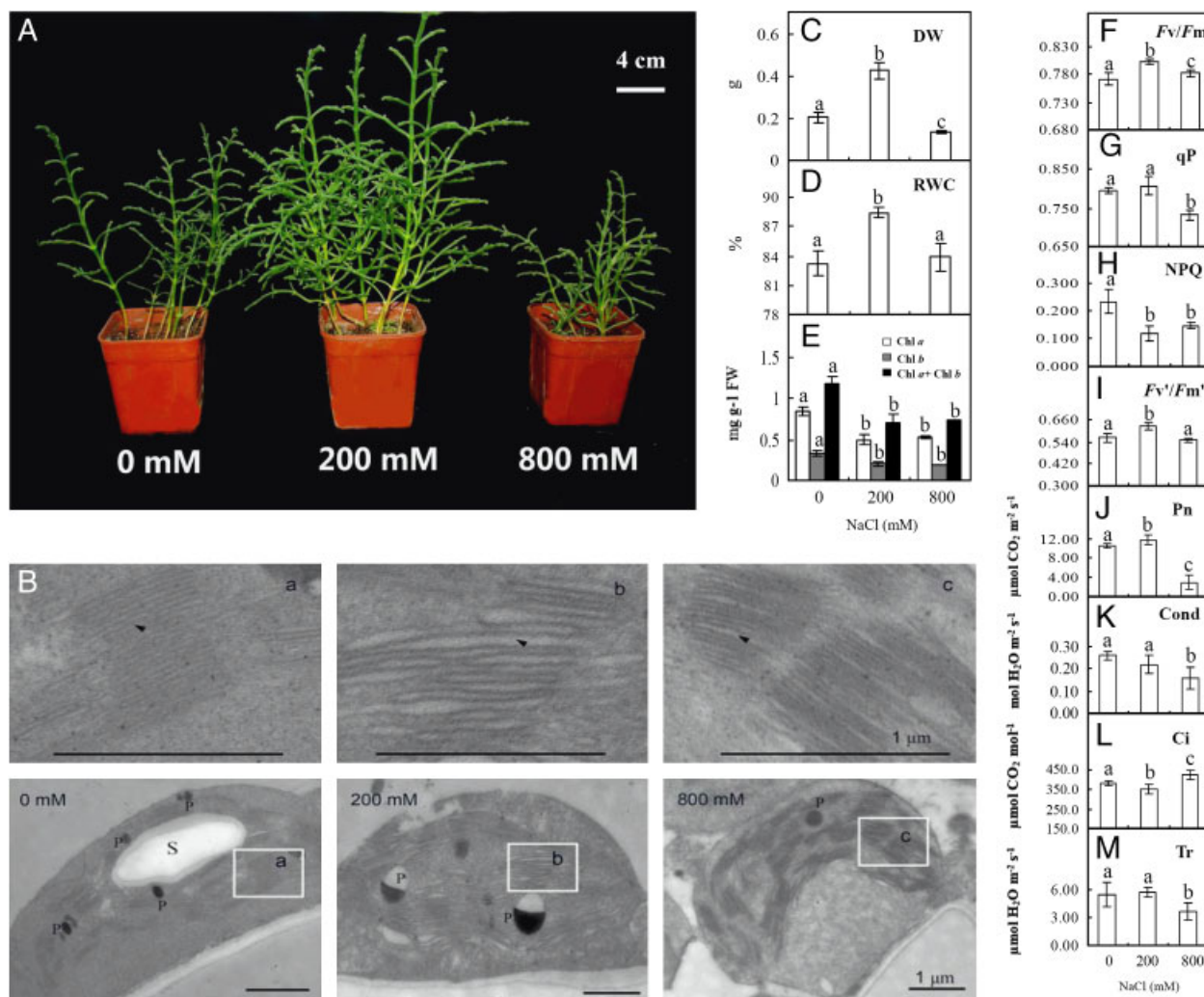


Figure 1. Effect of different salinity on photosynthesis parameters and chloroplast ultrastructure of *S. europaea*. (A) Seedlings that were 40 days old were treated with different concentrations of NaCl. The photographs were taken after 30 days of treatment. Scale bar equals to 4 cm. (B) Chloroplast ultrastructure in *S. europaea* treated with different concentrations of NaCl. The close-up image of thylakoid grana were pointed out by the framed regions, which were enlarged on the upper side. The arrows indicate lumens of thylakoid. Scale bars equal to 1 μm. S, starch; P, Plastoglobule. (C and D) The measurement of DW and RWC of *S. europaea* under different salinity. (E) The effect of salt treatment on chlorophyll content in *S. europaea*. (F–I) Changes in chlorophyll fluorescence parameters of maximum quantum efficiency of PSII (F_v/F_m) (F); photochemical quenching (q_P) (G); NPQ (H); the efficiency of excitation capture by open PSII centers (F_v'/F_m') (I) in *S. europaea* treated with different NaCl concentrations after 30 days. (J–M) Gas exchange parameters in P_n (J); Cond (K); C_i (L); T_r (M) in *S. europaea* plants treated with various NaCl concentrations for 30 days. The values are presented as mean \pm SD ($n = 6$). Different letters indicate means that are significantly different from each other ($p \leq 0.05$).

isolated chloroplasts was further evaluated by Western blotting with antibodies against proteins from different cell compartments to further confirm the purity of extracted chloroplast proteins. Tubulin and actin are two well-known cytoskeleton proteins found in all eukaryotic cells, which could be used as cytoplasmic protein markers, when inspecting the purity of isolated chloroplast [61]. Here we performed immunoblot analysis with anti- β -actin, which recognized proteins in the total protein extracts, but not in the chloroplast protein fraction (Fig. 2A). The analysis using antibody against nuclear located histone proteins H3

showed the same result as that of anti- β -actin. The plant PsbP, PsbO, and Lhcb2 proteins are located in thylakoid membrane, which are present and functional in PSII. Antibodies against PsbP, PsbO, and Lhcb2 recognized proteins from both the total protein extracts and the chloroplast protein fraction. In the meantime, the abundance of PsbP, PsbO, and Lhcb2 in the chloroplast protein fraction was increased by a large margin, indicating the efficient enrichment of the three proteins after the chloroplast extraction. These results prove that the chloroplast protein extracts were highly purified.

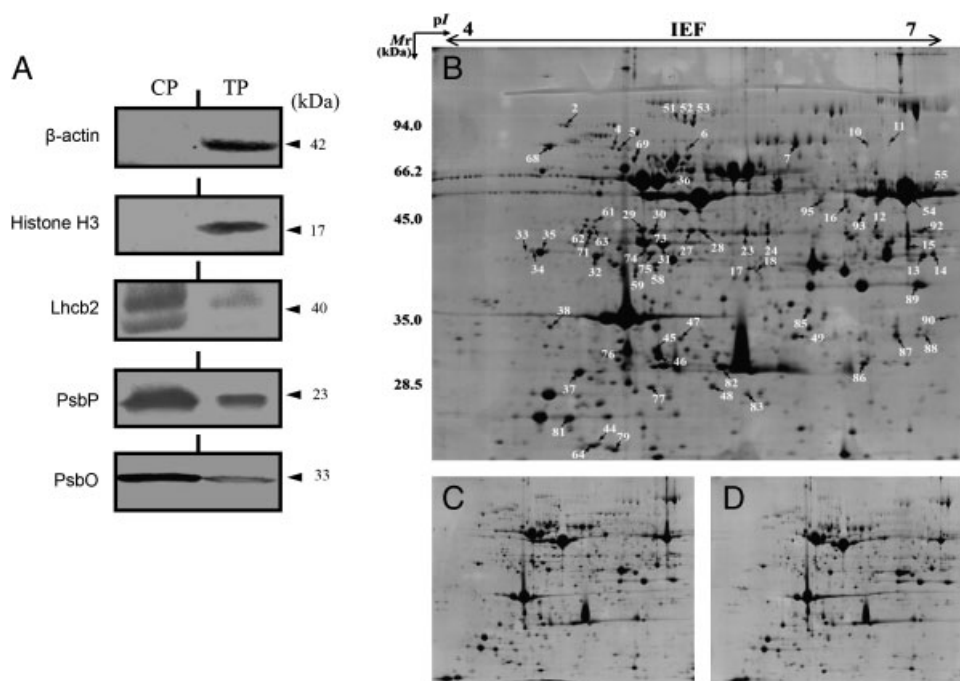


Figure 2. Purity assessment and representative 2-DE profiles of chloroplast proteins in *S. europaea*. (A) Western blot analysis of extracted chloroplast proteins with antibodies against proteins from different cell compartments. The immunoblot was carried out using antibodies against β -actin, Histone H3, PsbP, PsbO, and Lhcb2 to recognize proteins from both the total protein extracts (TP) and the chloroplast protein fraction (CP). (B) 2-DE profiles of proteins extracted from chloroplast of *S. europaea*. An equal amount (900 μ g) of total proteins was loaded on each gel strip (pH 4–7). After isoelectric focusing, 12.5% SDS-PAGE gels were used for second dimension separation. Protein spots were visualized using CBB staining. (B–D) are representative gels of chloroplast proteins for *S. europaea* treated with 0, 200, and 800 mM NaCl, respectively. The numbers of the 66 differentially expressed protein spots positively identified by nanoLC MS/MS are marked with arrows in (B).

3.4 Protein identification and functional classification

Chloroplast proteins extracted from *S. europaea* under different salinity were separated using 2-D gel electrophoresis. More than 1000 reproducible protein spots were determined among three biological repetitions for different treatments on each gel, as indicated in the three representative gel maps showed in Figs. 2B–D. With the global pattern of proteins largely remain unaltered, a total of 90 proteins (approximately 10% of total protein spots) were reproducibly detected as changed more than 1.5-fold in abundance and were significant statistically ($p \leq 0.05$). Furthermore, 66 out of the 90 differentially expressed proteins were positively identified by nanoLC MS/MS as listed in Table 1, with detailed information about matched peptides listed in Supporting Information Table S1. The subcellular location of identified proteins were predicted by the prediction tool TargetP [62]. Among them, 61 proteins were predicted to localize in chloroplast, one in mitochondria, and four in other localizations. It is likely that some proteins predicted by TargetP to localize in certain organelles might have dual-targeting compartments [63]. Nevertheless, the majority of the identified differential expressed proteins were predicted to be chloroplast-localized, indicating that the comparative

subcellular proteomics strategy could provide convincing results with the highly purified organelles.

To further examine the differentially expressed chloroplast proteins due to salt treatments, the identified proteins were grouped into 12 functional categories using the MapMan ontology as shown in Fig. 3A, including photosynthesis, oxidative pentose-phosphate pathway (OPP), ATP synthesis, lipid metabolism, N-metabolism, amino acid metabolism, S-assimilation, tetrapyrrole synthesis, redox, RNA regulation, protein metabolism, and proteins not yet with assigned function. Among the functional groups, the two major categories that involved in photosynthesis followed by protein metabolism were further classified into two and five sub-categories, which account for 37 and 31% of the total proteins, respectively.

Hierarchical clustering was conducted to the 66 identified proteins in order to visualize the coordinately regulated proteins and to cluster the proteins showing similar expression pattern under salt treatment. As shown in Fig. 3B, three main clusters were formed, as indicated by three representative protein spots. From the hierarchical cluster tree, we could clearly observe that many of the identified proteins including most of the enzymes involved in carbon assimilation, light reaction, and protein metabolism, increased in abundance under 200 mM NaCl condition.

Table 1. The differentially expressed *S. europaea* chloroplast proteins identified by nanoLC MS/MS and their relative volume changes under different salinity

Spot no. ^{a)}	Ac. no. ^{b)}	Protein name	Plant species	Theor. pI/Mr ^{c)}	Exper. pI/Mr ^{d)}	SC ^{e)}	M. score ^{f)}	TargetP ^{g)}	Relative V%±SD		
									0	200	800 ^{h)}
1 PS											
1.1 PS Light reaction											
37	20671	Chlorophyll <i>a/b</i> -binding protein	<i>Pisum sativum</i>	5.24/29	5.77/46	15	94	c			
45	430947	PSI type III chlorophyll <i>a/b</i> -binding protein	<i>Arabidopsis thaliana</i>	8.61/29	5.35/31	15	251	c			
46	110377793	Chloroplast pigment-binding protein CP26	<i>Nicotiana tabacum</i>	5.73/30	5.65/30	31	156	c			
48	217071344	Unknown (chlorophyll <i>a/b</i> -binding protein)	<i>Medicago truncatula</i>	6.59/31	5.87/27	13	337	c			
71	119906	Ferredoxin-NADP reductase, chloroplastic	<i>Spinacia oleracea</i>	8.67/41	4.97/48	12	172	c			
76	430947	PSI type III chlorophyll <i>a/b</i> -binding protein	<i>Arabidopsis thaliana</i>	8.61/29	5.04/31	17	202	c			
79	146403796	Chloroplast light-harvesting chlorophyll <i>a/b</i> -binding protein	<i>Artemisia annua</i>	5.32/27	5.04/16	34	114	c			
81	158935079	Rieske iron-sulfur protein precursor	<i>Glycine max</i>	9.01/25	4.33/25	13	223	c			
82	148535011	23 kDa OEC protein	<i>Salicornia veneta</i>	5.94/22	5.68/29	45	234	c			
83	225447691	Hypothetical protein (cytochrome <i>b6/f</i> complex)	<i>Vitis vinifera</i>	8.90/25	5.98/34	12	239	c			
89	20302471	Ferredoxin-NADP(H) oxidoreductase	<i>Triticum aestivum</i>	8.29/39	7.10/38	30	1883	c			
1.3 PS Calvin cycle											
7	118487947	Unknown (TK)	<i>Populus trichocarpa</i>	5.97/81	6.02/78	14	147	c			

Table 1. Continued

Spot no. ^{a)}	Ac. no. ^{b)}	Protein name	Plant species	Theor. pI/M _r ^{c)}	Exper. pI/M _r ^{d)}	SC ^{e)}	M. score ^{f)}	TargetP ^{g)}	Relative V% ± SD
									0 200 800 ^{h)}
13	77540210	Glyceraldehyde-3-phosphate dehydrogenase A subunit	<i>Glycine max</i>	8.42/43	7.32/44	25	808	c	
15	20455487	Glyceraldehyde-3-phosphate dehydrogenase A, chloroplastic	<i>Spinacia oleracea</i>	7.62/43	6.40/45	36	1320	c	
18	1351271	Triosephosphate isomerase, chloroplastic	<i>Spinacia oleracea</i>	6.45/35	5.96/42	21	242	c	
23	186491325	Phosphoglycerate kinase, putative	<i>Arabidopsis thaliana</i>	5.39/43	5.94/48	27	1446	c	
31	21950712	Rubisco activase	<i>Chenopodium quinoa</i>	6.56/48	5.77/46	46	2698	c	
32	3914940	Sedoheptulose-1,7-bisphosphatase, chloroplastic	<i>Spinacia oleracea</i>	5.87/43	4.68/44	17	256	c	
54	1050532	Ribulose-1,5-bisphosphate carboxylase	<i>Hillia triflora</i>	6.22/53	6.38/50	36	1988	c	
55	34576631	Ribulose-1,5-bisphosphate carboxylase/oxygenase large subunit	<i>Chenoleoides tomentosa</i>	6.13/50	7.0/51	41	592	c	
61	21950712	Rubisco activase	<i>Chenopodium quinoa</i>	6.56/48	4.91/49	31	790	c	
62	21950712	Rubisco activase	<i>Chenopodium quinoa</i>	6.56/48	4.79/49	27	323	c	
63	21950712	Rubisco activase	<i>Chenopodium quinoa</i>	6.56/48	4.97/49	27	786	c	
73	21950712	Rubisco activase	<i>Chenopodium quinoa</i>	6.56/48	5.47/46	36	814	c	
92	120665	Glyceraldehyde-3-phosphate dehydrogenase B, chloroplastic	<i>Nicotiana tabacum</i>	8.83/48	7.50/48	14	122	c	

Table 1. Continued

Spot no. ^{a)}	Ac. no. ^{b)}	Protein name	Plant species	Theor. p//M _r ^{c)}	Exper. p//M _r ^{d)}	SC ^{e)}	M. score ^{f)}	TargetP ^{g)}	Relative V% ± SD
									0 200 800 ^{h)}
7. OPP									
16	13936693	6PGDH	<i>Spinacia oleracea</i>	5.54/59	6.13/49	13	233	c	
9. ATP synthesis									
49	115472	Carbonic anhydrase, chloroplastic	<i>Spinacia oleracea</i>	6.61/35	6.03/31	19	147	c	
87	115472	Carbonic anhydrase, chloroplastic	<i>Spinacia oleracea</i>	6.61/35	6.34/31	28	795	c	
88	115472	Carbonic anhydrase, chloroplastic	<i>Spinacia oleracea</i>	6.61/35	7.57/31	19	223	c	
11. Lipid metabolism									
59	14422259	Enoyl-[acyl-carrier protein] reductase	<i>Brassica napus</i>	8.53/41	5.27/41	15	339	c	
24	56463275	Choline monooxygenase	<i>Salicornia europaea</i>	5.88/50	6.03/47	35	560	c	
12. N-Metabolism									
29	193290696	Putative glutamine synthase 2	<i>Capsicum annuum</i>	6.48/48	5.15/48	22	348	c	
30	193290696	Putative glutamine synthase 2	<i>Capsicum annuum</i>	6.48/48	5.69/48	29	758	c	
13. Amino acid metabolism									
12	1711381	Phosphoserine aminotransferase, chloroplastic	<i>Spinacia oleracea</i>	8.26/48	6.31/47	7	121	c	
47	303902	Cysteine synthase	<i>Spinacia oleracea</i>	6.79/41	5.80/32	21	264	c	
14. S-Assimilation									
93	255538896	Sulfate adenylyltransferase, putative	<i>Ricinus communis</i>	5.94/48	6.28/54	16	294	o	



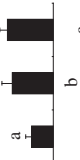


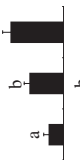


Table 1. Continued

Spot no. ^{a)}	Ac. no. ^{b)}	Protein name	Plant species	Theor. p//M _r ^{c)}	Exper. p//M _r ^{d)}	SC ^{e)}	M. score ^{f)}	TargetP ^{g)}	Relative V%±SD
									0 200 800 ^{h)}
19. Tetrapyrrole synthesis									
17	7431648	Coproporphyrinogen oxidase	<i>Arabidopsis thaliana</i>	7.67/41	5.95/45	14	104	c	
74	255558669	Porphobilinogen deaminase, putative	<i>Ricinus communis</i>	6.55/40	5.48/45	6	265	c	
21. Redox									
77	224082097	Predicted protein (ascorbate peroxidase)	<i>Populus trichocarpa</i>	5.75/37	5.51/27	9	277	o	
86	54292100	Manganese SOD	<i>Camellia sinensis</i>	7.82/26	6.16/28	24	128	m	
95	15320419	Monodehydroascorbate reductase	<i>Spinacia oleracea</i>	6.65/54	5.92/50	26	384	c	
27. RNA regulation									
14	1532135	Chloroplast mRNA-binding protein CSP41 precursor	<i>Spinacia oleracea</i>	6.11/45	7.13/44	20	277	c	
29. Protein									
29.2 Protein synthesis									
27	255540493	EF-Tu, putative	<i>Ricinus communis</i>	5.99/50	5.83/48	28	448	c	
28	1169494	EF-Tu, chloroplastic	<i>Glycine max</i>	6.33/53	5.85/48	12	341	c	
29.3 Protein targeting									
10	15232625	TOC75-III	<i>Arabidopsis thaliana</i>	8.93/90	6.30/77	6	85	c	
11	75221490	Protein TOC75, chloroplastic	<i>Pisum sativum</i>	7.01/89	6.35/77	4	141	c	

Table 1. Continued

Spot no. ^{a)}	Ac. no. ^{b)}	Protein name	Plant species	Theor. pI/M _r ^{c)}	Exper. pI/M _r ^{d)}	SC ^{e)}	M. score ^{f)}	TargetP ^{g)}	Relative V% ± SD
									0 200 800 ^{h)}
29.5 Protein degradation									
6	255539168	Cell division protease ftsH, putative	<i>Ricinus communis</i>	6.27/75	5.82/75	23	359	c	
36	75114857	Cell division protease ftsH homolog 2, chloroplastic	<i>Oryza sativa</i>	5.54/73	5.84/71	32	1429	c	
51	255540075	ATP-dependent clp protease, putative	<i>Ricinus communis</i>	6.27/103	5.81/105	11	163	c	
52	4105131	ClpC protease	<i>Spinacia oleracea</i>	8.78/100	5.86/104	41	669	c	
53	255540075	ATP-dependent clp protease, putative	<i>Ricinus communis</i>	6.27/103	5.84/104	30	941	c	
69	17865463	Cell division protease ftsH homolog, chloroplastic	<i>Medicago sativa</i>	5.64/76	5.32/75	7	231	c	
75	2565436	DegP protease precursor	<i>Arabidopsis thaliana</i>	6.00/46	5.56/44	4	627	c	
29.6 Protein folding									
2	3913786	Luminal-binding protein	<i>Spinacia oleracea</i>	5.03/74	4.99/103	20	369	o	
4	3913786	Luminal-binding protein	<i>Spinacia oleracea</i>	5.03/74	4.95/77	29	1787	o	
5	255575054	Heat shock protein, putative	<i>Ricinus communis</i>	5.07/71	5.07/77	25	599	c	
33	10720315	Peptidyl-prolyl cis-trans isomerase, chloroplastic	<i>Spinacia oleracea</i>	5.29/50	4.43/45	21	263	c	
34	10720315	Peptidyl-prolyl cis-trans isomerase, chloroplastic	<i>Spinacia oleracea</i>	5.29/50	4.49/45	24	455	c	

Table 1. Continued

Spot no. ^{a)}	Ac. no. ^{b)}	Protein name	Plant species	Theor. pI/Mr ^{c)}	Exper. pI/Mr ^{d)}	SC ^{e)}	M. score ^{f)}	TargetP ^{g)}	Relative V% ± SD
									0 200 800 ^{h)}
35	10720315	Peptidyl-prolyl <i>cis-trans</i> isomerase, chloroplastic	<i>Spinacia oleracea</i>	5.29/50	4.54/45	24	700	c	
68	1143427	Heat shock protein 70	<i>Cucumis sativus</i>	5.15/75	4.63/79	28	1025	c	
85	255548201	Peptidyl-prolyl <i>cis-trans</i> isomerase, putative	<i>Ricinus communis</i>	8.66/29	6.07/34	18	197	c	
90	255541858	Peptidyl-prolyl <i>cis-trans</i> isomerase B, ppib, putative	<i>Ricinus communis</i>	8.49/36	8.42/36	10	270	c	
<i>29.8 Protein assembly</i>									
58	148251625	Plastid high chlorophyll fluorescence 136 precursor	<i>Zea mays</i>	8.71/43	5.63/42	12	104	c	
35. Not assigned									
38	118488681	Unknown (pentapeptide domain containing protein)	<i>Populus trichocarpa</i>	6.67/34	4.34/34	7	92	c	
44	115482792	Hypothetical protein (pentapeptide domain containing protein)	<i>Oryza sativa</i>	7.49/25	4.96/23	13	266	c	
64	217071608	Unknown (pentapeptide domain containing protein)	<i>Medicago truncatula</i>	8.12/26	4.92/23	17	759	c	

a) Assigned spot number as indicated in Fig. 2B.
b) Database accession numbers according to NCBItr.
c) Theoretical mass (kDa) and pI of identified proteins were retrieved from the protein database.
d) Experimental mass (kDa) and pI of identified proteins. Experimental values were calculated with Image Master 2D Platinum Software and standard molecular mass markers.
e) Sequence coverage.
f) The MASCOT score reported after searching against the NCBItr database.
g) TargetP predicts the subcellular location of eukaryotic proteins, c, chloroplast; o, other location; m, mitochondria.
h) Mean of protein spot relative volume (V%) ± SD. Each spot volume value was divided by the sum of total spot volume values to obtain individual relative volumes of the detected spots.

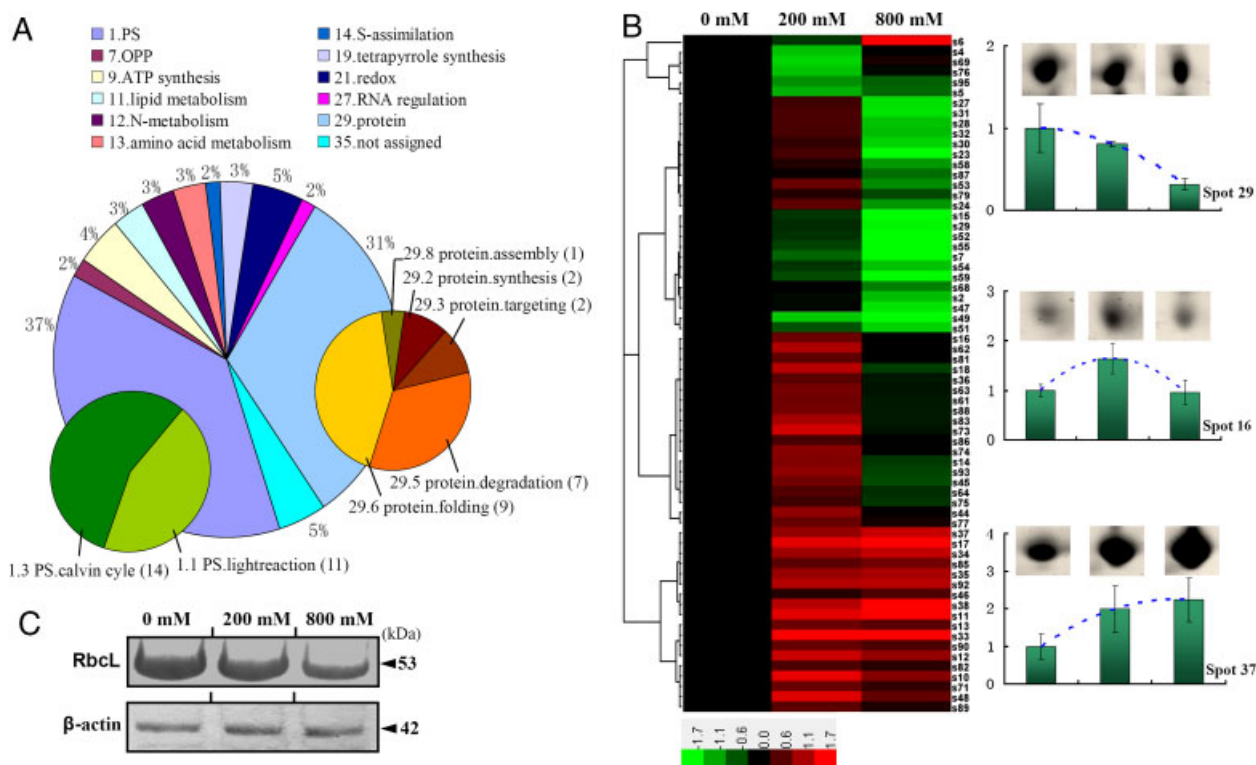


Figure 3. Functional classification and hierarchical clustering analysis of the 66 differentially expressed proteins. (A) Functional classification of the 66 identified proteins according to the MapMan ontology. The percentage of proteins from each class is shown. Two of the most abundant classes, photosynthesis and protein metabolism, were subsequently divided into two and four subgroups, respectively. (B) Hierarchical clustering analysis of expression profiles of the differentially expressed proteins. The three columns represent 0, 200, and 800 mM NaCl treatment, respectively. The rows represent individual proteins. The proteins increased and decreased in abundance are indicated in red and green, respectively. The intensity of the colors increases as the expression differences increase, as shown in the bar at the bottom. Of these proteins, three representative protein spots (spots 29, 16, 37) are shown on the right side. (C) Western blot analysis of RbcL in shoot of *S. europaea* under different salinity. Antibody against RbcL was applied for immunoblot analysis. β -actin was used as an internal loading control.

Western blot was performed to compare expression of *S. europaea* RbcL under different salinity (Fig. 3C). As RbcL is encoded by the chloroplast chromosome and synthesized in chloroplast, the total proteins extracted from aerial part of *S. europaea* were applied for the experiment using β -actin as internal control. The immunoblot analysis using antibodies against RbcL showed it slightly decreased in abundance under 200 mM NaCl treatment compared with non-saline condition, while its expression decreased significantly after exposure to 800 mM NaCl. The Western blot results agreed well with the quantification of the proteomics data for RbcL, indicating that the results of comparative proteomic study were convincing for further analysis.

3.5 Two-dimensional BN-PAGE analysis of thylakoid membrane proteins

Combining mild detergents and the dye CBB, BN-PAGE could efficiently separate intact protein complexes by apparent molecular mass, which also allows the separation

of protein complex in second dimensions for protein interactions [56]. BN-PAGE has become the preferred method to analyze the proteome of thylakoid membranes [64]. In our study, thylakoid membranes (with equal content of chlorophyll) were purified from 0, 200, and 800 mM NaCl-treated *S. europaea* plants. Then, they were solubilized in 1% DM followed by separation of BN-PAGE, in order to analyze the effect of salinity on thylakoid membrane proteins (Fig. 4A). The content of each protein complex for the three treatments were measured by the optical density of the band on the gels. The statistic results showed that band II and V had significant higher content for the 200 mM NaCl-treated plant than the other two treatments (Fig. 4B). After that, the thylakoid proteins from the lanes of the BN-PAGE gels were separated in the second dimension. Five protein spots from the position of band II and one protein from band V were excised and identified by nanoLC MS/MS, as indicated by arrows in Fig. 4C, with detailed identifications listed in Supporting Information Table S2. The results showed that thylakoid protein CP47, cytochrome *f*, D1 protein, as well as a chlorophyll *a/b* binding protein increased in abundance

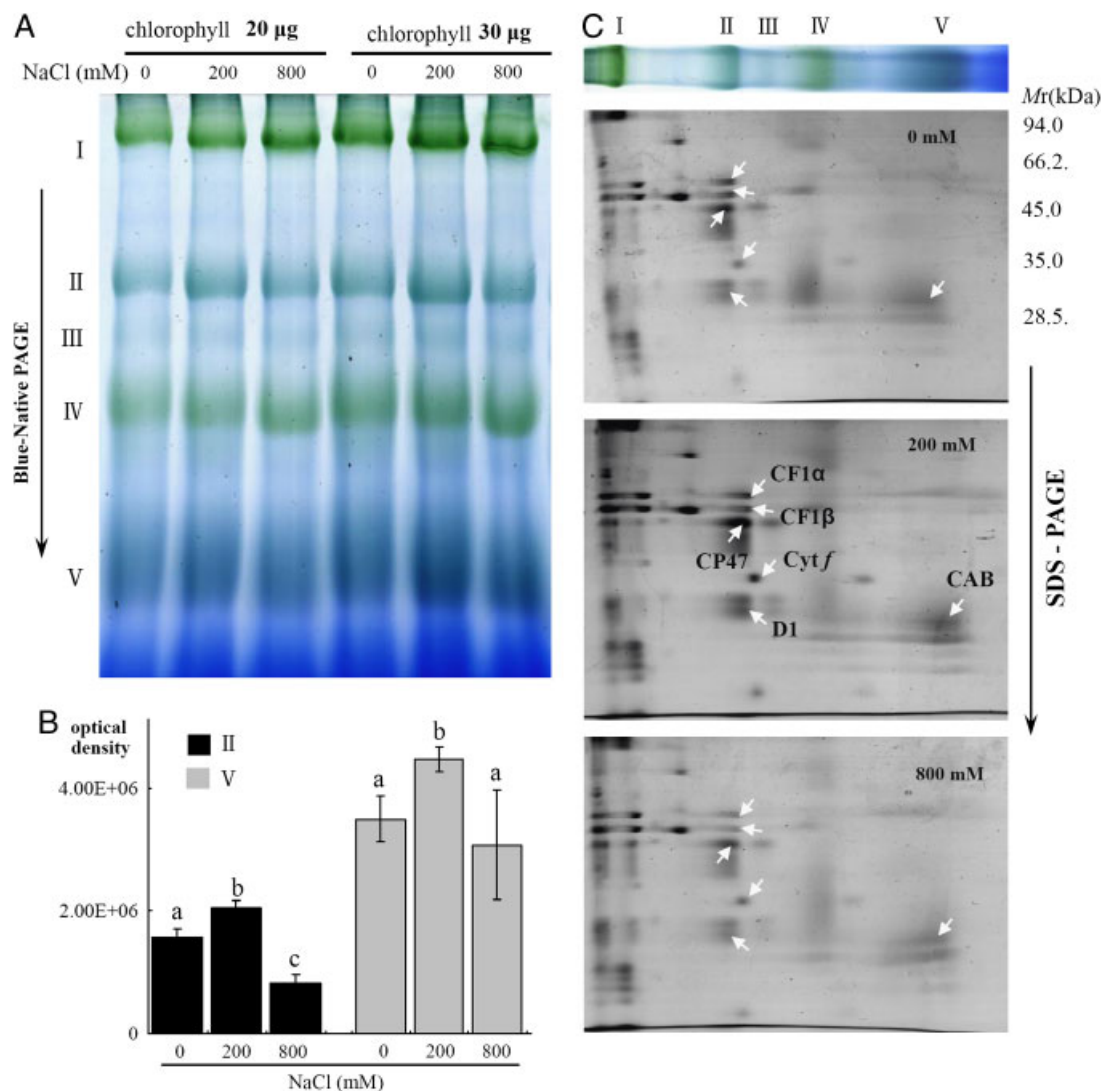


Figure 4. Analysis of thylakoid membrane proteins from different concentrations of NaCl-treated *S. europaea*. (A) BN-PAGE analysis of thylakoid membrane protein complexes. Thylakoid membranes isolated from 0, 200, and 800 mM NaCl-treated plants were solubilized with 1% DM and separated by BN-PAGE, with equal loading of 20 and 30 µg of chlorophyll, respectively. Five bands of protein complex for each lane were indicated by numbers on left side of the gel. (B) Semiquantitative analysis of thylakoid membrane protein complexes. The gels were scanned and analyzed using an Alphamager 2200 system. The content of the protein complexes were measured by optical density of the protein bands. The band intensities that have statistically significant different levels were showed. (C) Two-dimensional separation of protein complexes in the thylakoid membranes. BN-PAGE-separated thylakoid proteins in a single lane from a BN gel were separated in a second dimension by 12.5% SDS-PAGE and stained with CBB. The identities of six protein spots from the position of band II and V are indicated by arrows.

under 200 mM NaCl treatment, while the relative level of all the six proteins including CF1α and CF1β decreased drastically after high concentration of NaCl treatment.

3.6 Transcript analysis and correlation with proteomic data

Research into gene expression and proteomics will help to decipher the functions of genes and their protein products, and to get a clearer picture of the complex regulatory

networks that control fundamental biological processes. In our experiment, 12 key enzymes involved in Calvin cycle and other functional categories were analyzed in transcriptional level. As non-model plant, *S. europaea* does not have available genome or transcriptome sequence data for designing primers of a given gene. To overcome this difficulty, we searched for homologs of the selected identified proteins, designed degenerate primers by Consensus Degenerate Hybrid Oligonucleotide Primers from protein multiple sequence alignments, and then obtained EST of the selected protein genes by sequencing the PCR products

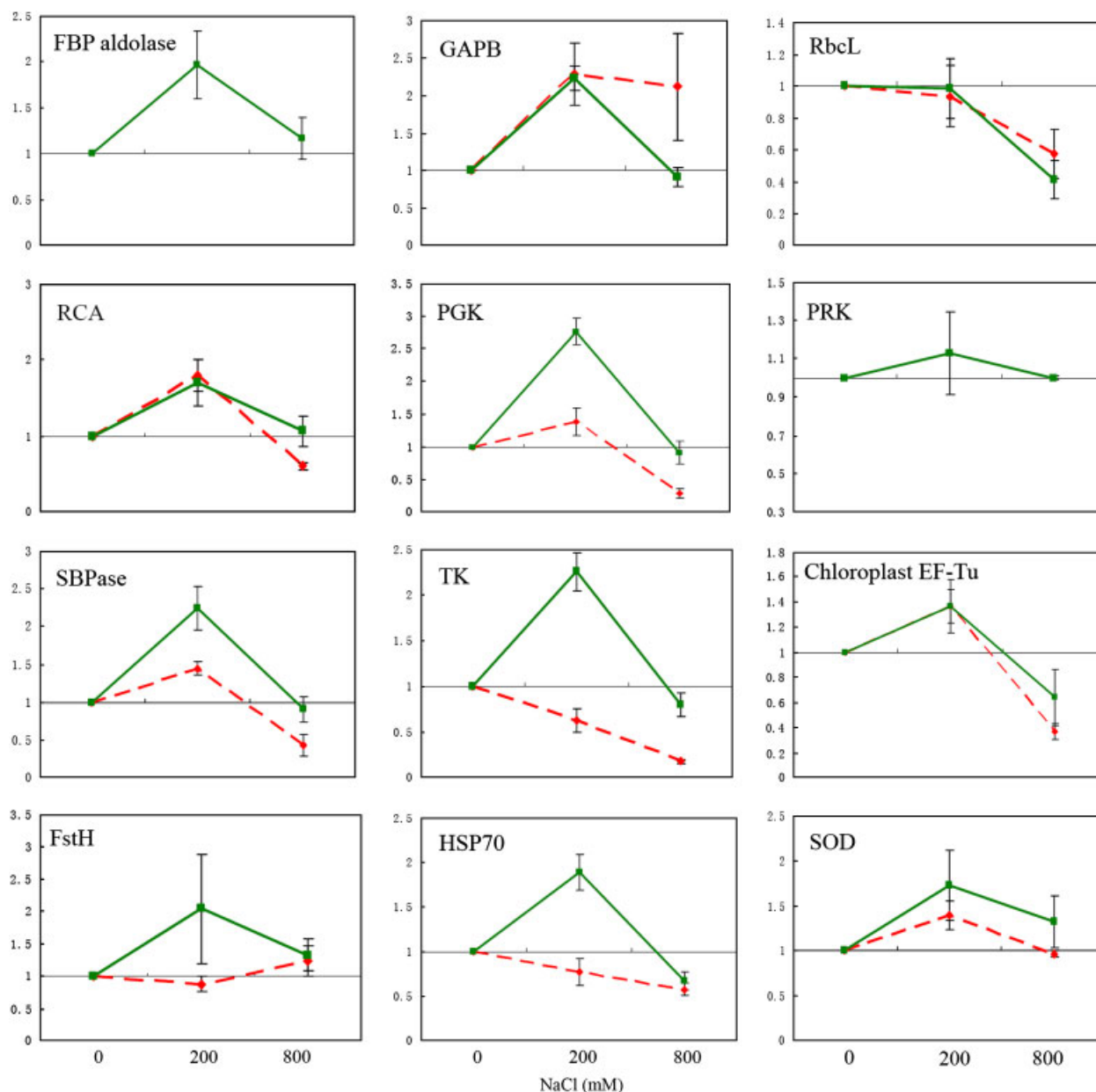


Figure 5. Comparison between expression profiles of protein-mRNA pairs of the selected protein-encoding genes after different concentration of NaCl treatment. The expression data of proteins were from relative volume (RV) of protein spots through the gel image analysis. The total RV of putative isoforms, three FtsH proteases (spot 6, 36, 69), five RCAs (spot 31, 61, 62, 63, 73), two RbcLs (spot 54 and spot 55), two EF-Tu (spot 27 and spot 28), and two HSP 70 (spot 5 and spot 68) were calculated and used for analysis. mRNA levels were evaluated by qRT-PCR. Standard deviation shown is averaged over three independent biological replicate samples for each treatment. The RV and $2^{-\Delta\Delta Ct}$ were selected to represent the expression of proteins and mRNA, respectively. Then, the data were normalized to fold change compared with non-saline condition. FBP aldolase and PRK, which were not detected in proteomic analysis, were only presented with mRNA expression data. The curves '—' and '---' represent mRNA and protein expression data, respectively.

of conserved cDNA regions. After that, quantitative RT-PCR (qRT-PCR) was carried out using primers designed from the EST as listed in Supporting Information Table S3.

As shown in Fig. 5, the normalized fold changes of both the gene expression level as well as the abundance of the corresponding proteins were compared in the same

diagram. Of the enzymes in Calvin cycle, RbcL, seduheptulose biphosphatase, RuBisCO activase (RCA), and phosphoglycerate kinase displayed similar protein and gene expression changing patterns under NaCl treatment, while transketolase (TK), glyceraldehyde-3-phosphate dehydrogenase subunit B, FtsH, and HSP70 showed different

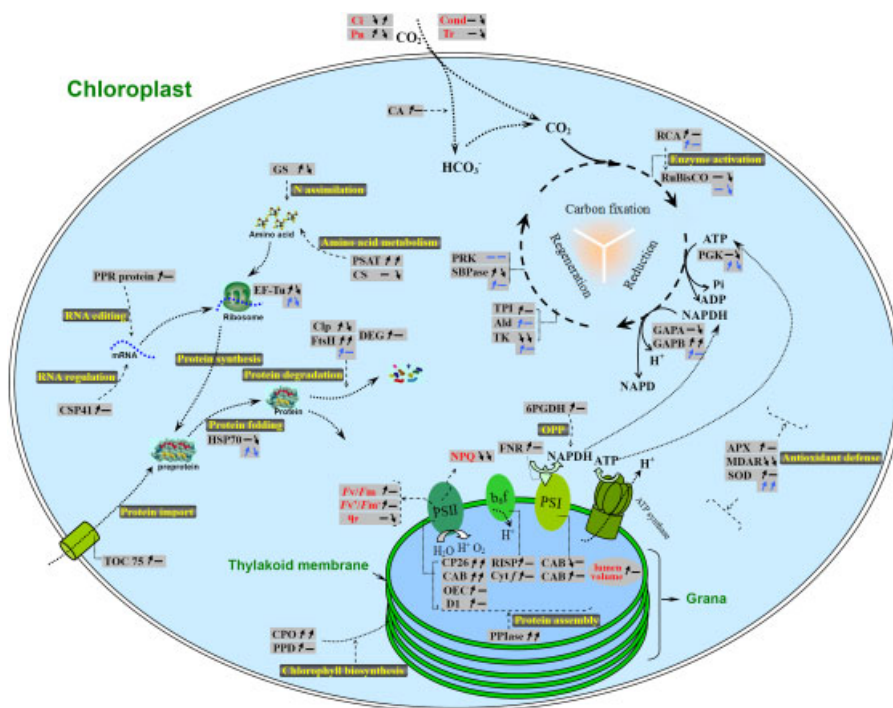


Figure 6. A putative model of photosynthesis network of *S. europaea* under salinity. Most of the identified proteins and the measured physiological parameters were integrated in the gray box of this figure, which were marked in black and red, respectively. The changed pattern of the proteins and the physiological parameters for 200 and 800 mM NaCl-treated plant were marked with symbols on the left and the right side of the gray box, respectively. The symbols are: increase in abundance, '▲'; decrease in abundance, '▼'; unchanged pattern, '—'. Meanwhile, the symbols in blue color indicate the mRNA changing pattern of the protein-encoding genes. The biological functions that the proteins might involve in were marked in yellow color in the black box. The evidence suggests that chloroplast proteins participate in Calvin cycle, light reaction, and nitrogen metabolism are critical in governing salt tolerance of *S. europaea*. Abbreviations not mentioned before are as follows, Ald, aldolase; APX, ascorbate peroxidase; CA, carbonic anhydrase; CAB, chlorophyll *a/b* bind proteins; CPO, coproporphyrinogen oxidase; CS, cysteine synthase; CSP41, chloroplast mRNA-binding protein CSP41 precursor; cyt *f*, cytochrome *f*; GS, glutamine synthetase; MDAR, monodehydroascorbate reductase; PPD, porphobilinogen deaminase; PSAT, phosphoserine amino-transferase; RISP, Rieske iron-sulfur protein; TOC 75, 75 kDa translocon at the outer-envelope membrane of chloroplasts; TRI, triose-phosphate isomerase.

trends. The transcript levels of superoxide dismutase (SOD), chloroplast elongation factor Tu (EF-Tu), displayed an increasing pattern under 200 mM NaCl treatment, which also showed similar trends with the proteomics data. Furthermore, in order to get a clearer image of the carbon assimilation network, we monitored the gene expression of another two important enzymes in the Calvin cycle, Fructose-bisphosphate (FBP) aldolase, and phosphoribulokinase (PRK), which were not identified in our proteomics study.

4 Discussion

Halophytes could tolerate a wide range of salinity and maintain relatively high growth rate at intermediate salinity, indicating their photosynthesis activity was under positive condition [21, 65, 66]. Different from glycophytes, the growth of *S. europaea* would be constrained under both non-saline condition and supra-optimal saline environment, and be promoted under moderate salinity. Based on

photosynthesis characterization, chloroplast ultrastructure observation, analysis of the chloroplast protein by 2-DE and BN-PAGE, as well as previously published results of the functions for the identified differentially expressed proteins, a possible regulatory photosynthesis network for *S. europaea* under moderate and high salinity was proposed (Fig. 6). From the schematic illustration, it is notable that many proteins were differentially regulated to facilitate the coordination of carbon fixation and nitrogen metabolism in chloroplast of *S. europaea* under salinity.

Reduction in photosynthesis of plant under stress conditions can be due to a range of factors that have been grouped into two categories, the CO₂ diffusion through the stomata to the fixation site and the biochemical or metabolic capacity of leaves to fix CO₂, which are often termed as stomatal limitation and non-stomatal limitation, respectively [67–69]. In our study, a negative correlation was observed between Ci and Pn. The reduction of photosynthesis for the 0 and 800 mM NaCl-treated plants is more likely due to the non-stomatal limitation, which might be caused by changes

in the enzymes associate with photosynthetic carbon metabolic pathway that occurred in chloroplast. Furthermore, the ultrastructure of chloroplasts observed for the 800 mM NaCl treatment remained intact without disintegrating, indicating that the photosynthesis reduction of *S. europaea* under high salinity is more likely due to the biochemical changes in the chloroplast other than damage of the photosynthetic apparatus. After all, the photosynthesis changes in halophytes under different salinity could be well elucidated by investigating the biochemical network alterations inside the chloroplast.

In thylakoid membrane, the PSII light-harvesting system consists of many chlorophyll *a/b* binding proteins, which carry out two essential functions, the efficient collection of light energy for photosynthesis and the regulated dissipation of excitation energy in excess of that which can be used [45, 70, 71]. This dual function requires flexibility of light-harvesting proteins that respond to environmental change. In our research, the results from comparative 2-DE of chloroplast protein correlated well with the analysis of membrane proteins by BN-PAGE, a method for quantification study of thylakoid associated photosynthesis protein complexes in plants [72, 73], which together proved that the relative level of many important proteins in the thylakoid membranes increased in abundance under 200 mM NaCl treatment compared with the non-saline or supra-optimal salinity condition. For example, the PSII antenna protein CP29 and CP47, as well as several chlorophyll *a/b* bind proteins in the PSII and PSI light harvest system showed increased abundance under salt treatment, with only one protein decreased, which was consistent with the increment of *Fv/Fm*, as well as *Fv'/Fm'* under 200 mM NaCl treatment, indicating that moderate salt treatment to *S. europaea* could enhance the excitation energy capturing ability and efficiency of PSII. Meanwhile, Rieske iron-sulfur protein and cytochrome *f*, components of the cytochrome *b₆/f* complex, as well as two ferredoxin-nicotinamide adenine dinucleotide phosphate (NADP⁺) reductases, were observed increasing in abundance in 200 mM NaCl-treated *S. europaea*. Cytochrome *b₆/f* complex participates in electron transferring between PSI and PSII, and plays an important role in transmembrane electrochemical proton gradient formation by transferring protons from the stroma to the lumen compartment, which result in ATP production [74]. Ferredoxin-NADP⁺ reductase was reported to bound peripherally to PSI and is implicated in generating NADPH (the reduced form of NADP⁺) for reducing power [74, 75]. The increment of the above thylakoid proteins suggested that light reaction was active for *S. europaea* under moderate salinity, which generated more energy and reduced power for carbon and nitrogen assimilation. Interestingly, the chlorophyll content of *S. europaea* decreased after irrigation with salt water, which might be due to the substantial increase of RWC of shoots after salt treatment.

An important mechanism for coordination of carbon and nitrogen metabolism in *S. europaea* under salinity was revealed in our study by the different regulated key enzymes

involved in carbon/nitrogen metabolic process. In the experiment, the chloroplast envelop membrane protein carbonic anhydrase was increased in abundance under 200 mM NaCl treatment, which helped raise CO₂ concentration within the chloroplast, thus increasing the carboxylation rate of RuBisCO [76]. As an enzyme involved in the Calvin cycle that catalyzes the primary step of carbon fixation, RuBisCO showed similar protein and gene expression levels both under moderate salinity and non-saline conditions, while it decreased in abundance under high salinity. At the same time, RCA, which helps convert RuBisCO from its inactive form to active state, increased in abundance under 200 mM NaCl condition. The results implicated that there might be more RuBisCO in active form under moderate salinity than non-saline condition, which increased the carboxylation rate of CO₂. The changed state of enzyme involved in carbon assimilation inside the chloroplast might explain the negative correlation of *Ci* and *Pn* under salinity. Several enzymes involved in Calvin cycle other than RuBisCO were also changed in abundance, which could affect carbon assimilation. Phosphoglycerate kinase and glyceraldehyde-3-phosphate dehydrogenase subunit B, which catalyze major steps in the reduction stage by consuming ATP and NADPH, were increased in abundance under moderate salinity and decreased under high salinity. Triosephosphate isomerase, seduheptulose biphosphatase, TK, and FBP aldolase, which involved in regeneration step of Calvin cycle, also showed increased protein or gene expression level under salinity, suggesting that the regenerative step of Calvin cycle could be accelerated under moderate salinity, thus providing more ribulose-1, 5-bisphosphate to initiate a new cycle. Moreover, the qRT-PCR assay showed little change on the gene expression level of PRK under salinity, suggesting that the last step of Calvin cycle might not be affected for *S. europaea* plant under salinity condition. The elevated carbon assimilation as well as the reducing power produced during the process could facilitate the nitrogen use efficiency of plant [77, 78]. As a critical nutrition required by plants, the assimilated nitrogen could in turn support the use of CO₂ to produce the basic building blocks of biomass accumulation, such as sugars, organic acids, amino acids, nucleotides, chlorophylls, and numerous other metabolic components [77]. In our study, two glutamine synthases, which play essential roles by catalyzing the condensation of glutamate and ammonia to form glutamine [79], increased in abundance in 200 mM NaCl-treated plant, suggesting the ability of nitrogen assimilation in chloroplast of *S. europaea* was enhanced under moderate salinity.

It has been recognized that the better coordination of carbon and nitrogen assimilation could also facilitate proteins synthesis and other metabolic process [77]. In our study, the increment of two proteins under salinity, coproporphyrinogen oxidase, and porphobilinogen deaminase, which involved in tetrapyrrole synthesis [80], might facilitate producing more chlorophylls by consuming of both carbon

and nitrogen source. The pentatricopeptide-containing protein in *S. europaea* increased in abundance under salinity to help RNA editing in chloroplast [81]. At the same time, the chloroplast mRNA-binding protein CSP41 precursor increased in abundance, which might help to regulate transcription and translation of chloroplast-encoded RNAs under moderate salinity [82]. The increment of EF-Tu helped initiation and elongation of the freshly synthesized peptide chains, which could compensate for the large turnover of proteins in chloroplast. Two protein translocation channel, 75 kDa translocon at the outer-envelope membrane of chloroplasts, were shown to increase in abundance under salinity, which could help importing nuclear-encoded preproteins to their targets at chloroplast [83]. The elevated expression of HSP70 and luminal-binding protein could help fold the newly synthesized or imported protein precursors, while the increased ATP-dependent Clp protease, DegP protease, and FtsH protease could assist in degradation of the obsolete protein within chloroplasts [84]. In thylakoid lumen, many thylakoid membrane proteins also exist in the lumen in an unassembled state, in which they are long lived and assembly-competent [85]. Peptidylprolyl *cis-trans* isomerases, a big group of thylakoid lumen proteins, participating in maintenance of PSII through the protection of the unassembled proteins and in their proper assembly to PSII [86, 87], increased in abundance under moderate salinity, indicating a large turnover of proteins also exists in thylakoid lumen. The observed swollen of thylakoid lumen under 200 mM NaCl treatment might provide more space for the protein turnover process, which also reflect the active state of protein metabolism inside the compartment. After all, the changing patterns of all the enzymes involved in protein metabolism indicate an active quality control system of proteins exist in chloroplasts, which play an important role in modulating the photosynthesis network of *S. europaea* under salinity condition.

Three antioxidant proteins, ascorbate peroxidase, SOD, and monodehydroascorbate reductase, which play important roles in protecting plant cells against the oxidative damages induced by ROS, were also identified as differentially expressed proteins in our experiment, which was consistent with the results of *Suaeda salsa*, another C_3 halophyte [24, 25]. Interestingly, the different changing patterns between monodehydroascorbate reductase and the other two antioxidant enzyme might indicate their different roles in the chloroplast of salt-treated *S. europaea*. Plastidic 6-phosphogluconate dehydrogenase (6PGDH), an enzyme of the non-oxidative phase of the OPP, increased in abundance in 200 mM NaCl-treated plant. The increased expression of 6PGDH under moderate salinity might accelerate OPP, which is thought to generate large amounts of reducing power and metabolic intermediates to drive various anabolic processes [88].

In addition, our results also displayed that 41 of the 66 identified proteins appeared to be 14 unique kinds of

proteins, suggesting these sets of proteins might be isoforms due to the PTM of a protein or belong to the same protein families. Their expression profile patterns were compared as displayed in Supporting Information Fig. S1. These findings provided evidence on how the isoforms or family proteins in chloroplast modulate the photosynthesis network of *S. europaea* under different salinity.

*This research was supported by Research Program from the Chinese Ministry of Agriculture (Grant No. 2009ZX08009-101B), the Knowledge Innovation Project of Chinese Academy of Sciences (Grant No. KSCX2-EW-J-1), and the National High Technology and Research Development Program of China ("863" project) (Grant No. 2007AA091705). The authors thank Dafeng Jinglong Marine Industrialized Development Corporation, Ltd., Jiangsu Province for providing seeds of *S. europaea*.*

The authors have declared no conflict of interest.

5 References

- [1] Apse, M. P., Aharon, G. S., Snedden, W. A., Blumwald, E., Salt tolerance conferred by overexpression of a vacuolar Na^+/H^+ antiport in Arabidopsis. *Science* 1999, 285, 1256–1258.
- [2] Munns, R., Physiological processes limiting plant-growth in saline soils - some dogmas and hypotheses. *Plant Cell Environ.* 1993, 16, 15–24.
- [3] Munns, R., Schachtman, D. P., Condon, A. G., The significance of a two-phase growth response to salinity in wheat and barley. *Aust. J. Plant Physiol.* 1995, 22, 561–569.
- [4] Flowers, T. J., Improving crop salt tolerance. *J. Exp. Bot.* 2004, 55, 307–319.
- [5] Hasegawa, M., Bressan, R., Pardo, J. M., The dawn of plant salt tolerance genetics. *Trends Plant Sci.* 2000, 5, 317–319.
- [6] Hasegawa, P. M., Bressan, R. A., Zhu, J. K., Bohnert, H. J., Plant cellular and molecular responses to high salinity. *Annu. Rev. Plant Physiol. Mol. Biol.* 2000, 51, 463–499.
- [7] Zhu, J. K., Plant salt tolerance. *Trends Plant Sci.* 2001, 6, 66–71.
- [8] Zhu, J. K., Salt and drought stress signal transduction in plants. *Annu. Rev. Plant Biol.* 2002, 53, 247–273.
- [9] Muranaka, S., Shimizu, K., Kato, M., A salt-tolerant cultivar of wheat maintains photosynthetic activity by suppressing sodium uptake. *Photosynthetica* 2002, 40, 509–515.
- [10] Robinson, S. P., Downton, W. J. S., Millhouse, J. A., Photosynthesis and ion content of leaves and isolated-chloroplasts of salt-stressed spinach. *Plant Physiol.* 1983, 73, 238–242.
- [11] Ball, M. C., Farquhar, G. D., Photosynthetic and stomatal responses of the grey mangrove, *Avicennia-marina*, to transient salinity conditions. *Plant Physiol.* 1984, 74, 7–11.
- [12] Hichem, H., Naceur, E. A., Mounir, D., Effects of salt stress on photosynthesis, PSII photochemistry and thermal energy dissipation in leaves of two corn (*Zea mays* L.) varieties. *Photosynthetica* 2009, 47, 517–526.

- [13] Lu, K. X., Cao, B. H., Feng, X. P., He, Y. et al., Photosynthetic response of salt-tolerant and sensitive soybean varieties. *Photosynthetica* 2009, 47, 381–387.
- [14] Mehta, P., Jajoo, A., Mathur, S., Bharti, S., Chlorophyll *a* fluorescence study revealing effects of high salt stress on Photosystem II in wheat leaves. *Plant Physiol. Biochem.* 2010, 48, 16–20.
- [15] Stepien, P., Johnson, G. N., Contrasting responses of photosynthesis to salt stress in the glycophyte *Arabidopsis* and the halophyte *Thellungiella*: role of the plastid terminal oxidase as an alternative electron sink. *Plant Physiol.* 2009, 149, 1154–1165.
- [16] Tiwari, B. S., Bose, A., Ghosh, B., Photosynthesis in rice under a salt stress. *Photosynthetica* 1997, 34, 303–306.
- [17] Yamane, K., Rahman, S., Kawasaki, M., Taniguchi, M. et al., Pretreatment with antioxidants decreases the effects of salt stress on chloroplast ultrastructure in rice leaf segments (*Oryza sativa* L.). *Plant Prod. Sci.* 2004, 7, 292–300.
- [18] Zheng, C. F., Jiang, D., Liu, F. L., Dai, T. B. et al., Effects of salt and waterlogging stresses and their combination on leaf photosynthesis, chloroplast ATP synthesis, and antioxidant capacity in wheat. *Plant Sci.* 2009, 176, 575–582.
- [19] Li, N. Y., Chen, S. L., Zhou, X. Y., Li, C. Y. et al., Effect of NaCl on photosynthesis, salt accumulation and ion compartmentation in two mangrove species, *Kandelia candel* and *Bruguiera gymnorhiza*. *Aquat. Bot.* 2008, 88, 303–310.
- [20] Flowers, T. J., Colmer, T. D., Salinity tolerance in halophytes. *New Phytol.* 2008, 179, 945–963.
- [21] Redondo-Gomez, S., Mateos-Naranjo, E., Figueroa, M. E., Davy, A. J., Salt stimulation of growth and photosynthesis in an extreme halophyte, *Arthrocnemum macrostachyum*. *Plant Biol.* 2010, 12, 79–87.
- [22] Qiu, N., Lu, C., Enhanced tolerance of photosynthesis against high temperature damage in salt-adapted halophyte *Atriplex centralasiatica* plants. *Plant Cell Environ.* 2003, 26, 1137–1145.
- [23] Qiu, N. W., Lu, Q. T., Lu, C. M., Photosynthesis, photosystem II efficiency and the xanthophyll cycle in the salt-adapted halophyte *Atriplex centralasiatica*. *New Phytol.* 2003, 159, 479–486.
- [24] Pang, C. H., Zhang, S. J., Gong, Z. Z., Wang, B. S., NaCl treatment markedly enhances H₂O₂-scavenging system in leaves of halophyte *Suaeda salsa*. *Physiol. Plant.* 2005, 125, 490–499.
- [25] Zhang, Q. F., Li, Y. Y., Pang, C. H., Lu, C. M. et al., NaCl enhances thylakoid-bound SOD activity in the leaves of *C₃* halophyte *Suaeda salsa* L. *Plant Sci.* 2005, 168, 423–430.
- [26] Gatto, L., Vizcaino, J. A., Hermjako, H., Huber, W. et al., Organelle proteomics experimental designs and analysis. *Proteomics* 2010, 10, 3957–3969.
- [27] Qin, G. Z., Meng, X. H., Wang, Q., Tian, S. P., Oxidative damage of mitochondrial proteins contributes to fruit senescence: a redox proteomics analysis. *J. Proteome Res.* 2009, 8, 2449–2462.
- [28] Pandey, A., Chakraborty, S., Datta, A., Chakraborty, N., Proteomics approach to identify dehydration responsive nuclear proteins from chickpea (*Cicer arietinum* L.). *Mol. Cell. Proteomics* 2008, 7, 88–107.
- [29] Zhang, L. F., Yang, H. M., Cui, S. X., Hu, J. et al., Proteomic analysis of plasma membranes of *Cyanobacterium Synechocystis* sp strain PCC 6803 in response to high pH stress. *J. Proteome Res.* 2009, 8, 2892–2902.
- [30] Baginsky, S., Reiland, S., Grossmann, J., Baerenfaller, K. et al., Integrated proteome and metabolite analysis of the de-etiolation process in plastids from rice (*Oryza sativa* L.). *Proteomics* 2011, 11, 1751–1763.
- [31] Zorb, C., Herbst, R., Forreiter, C., Schubert, S., Short-term effects of salt exposure on the maize chloroplast protein pattern. *Proteomics* 2009, 9, 4209–4220.
- [32] Zhou, Y. J., Gao, F., Li, X. F., Zhang, J. et al., Alterations in phosphoproteome under salt stress in *Thellungiella* roots. *Chinese Sci. Bull.* 2010, 55, 3673–3679.
- [33] Pang, Q. Y., Chen, S. X., Dai, S. J., Chen, Y. Z. et al., Comparative proteomics of salt tolerance in *Arabidopsis thaliana* and *Thellungiella halophila*. *J. Proteome Res.* 2010, 9, 2584–2599.
- [34] Gao, F., Zhou, Y. J., Huang, L. Y., He, D. C. et al., Proteomic analysis of long-term salinity stress-responsive proteins in *Thellungiella halophila* leaves. *Chinese Sci. Bull.* 2008, 53, 3530–3537.
- [35] Askari, H., Edqvist, J., Hajheidari, M., Kafi, M. et al., Effects of salinity levels on proteome of *Suaeda aegyptiaca* leaves. *Proteomics* 2006, 6, 2542–2554.
- [36] Ungar, I. A., Population characteristics, growth, and survival of the halophyte *Salicornia europaea*. *Ecology* 1987, 68, 569–575.
- [37] Ushakova, S. A., Kovaleva, N. P., Tikhomirova, N. A., Gribovskaya, I. V. et al., Effect of photosynthetically active radiation, salinization, and type of nitrogen nutrition on growth of *Salicornia europaea* plants. *Russian J. Plant Physiol.* 2006, 53, 785–792.
- [38] Tikhomirova, N. A., Ushakova, S. A., Kovaleva, N. P., Gribovskaya, I. V. et al., Influence of high concentrations of mineral salts on production process and NaCl accumulation by *Salicornia europaea* plants as a constituent of the LSS phototroph link. *Adv. Space Res.* 2005, 35, 1589–1593.
- [39] Ushakova, S. A., Kovaleva, N. P., Gribovskaya, T. V., Dolgushev, V. A. et al., Effect of NaCl concentration on productivity and mineral composition of *Salicornia europaea* as a potential crop for utilization NaCl in LSS. *Adv. Space Res.* 2005, 36, 1349–1353.
- [40] Wang, X. C., Fan, P. X., Song, H. M., Chen, X. Y. et al., Comparative proteomic analysis of differentially expressed proteins in shoots of *Salicornia europaea* under different salinity. *J. Proteome Res.* 2009, 8, 3331–3345.
- [41] Drake, B. G., Photosynthesis of salt-marsh species. *Aquat. Bot.* 1989, 34, 167–180.
- [42] Johnson, B. J., Moore, K. A., Lehmann, C., Bohlen, C. et al., Middle to late holocene fluctuations of *C₃* and *C₄* vegetation in a Northern New England salt marsh, Sprague Marsh, Phippsburg Maine. *Org. Geochem.* 2007, 38, 394–403.

- [43] Shomerilan, A., Nissenbaum, A., Waisel, Y., Photosynthetic pathways and the ecological distribution of the Chenopodiaceae in Israel. *Oecologia* 1981, **48**, 244–248.
- [44] Porra, R. J., Thompson, W. A., Kriedemann, P. E., Determination of accurate extinction coefficients and simultaneous equations for assaying chlorophylls *a* and *b* extracted with four different solvents: verification of the concentration of chlorophyll standards by atomic absorption spectroscopy. *Biochim. Biophys. Acta* 1989, **975**, 384–394.
- [45] Baker, N. R., Chlorophyll fluorescence: a probe of photosynthesis in vivo. *Annu. Rev. Plant Biol.* 2008, **59**, 89–113.
- [46] Maxwell, K., Johnson, G. N., Chlorophyll fluorescence - A practical guide. *J. Exp. Bot.* 2000, **51**, 659–668.
- [47] Fan, P. X., Wang, X. C., Kuang, T. Y., Li, Y. X., An efficient method for the extraction of chloroplast proteins compatible for 2-DE and MS analysis. *Electrophoresis* 2009, **30**, 3024–3033.
- [48] Bradford, M. M., Rapid and sensitive method for quantitation of microgram quantities of protein utilizing principle of protein-dye binding. *Anal. Biochem.* 1976, **72**, 248–254.
- [49] Wang, X. C., Li, X. F., Li, Y. X., A modified Coomassie Brilliant Blue staining method at nanogram sensitivity compatible with proteomic analysis. *Biotechnol. Lett.* 2007, **29**, 1599–1603.
- [50] Wang, X. C., Li, X. F., Deng, X., Han, H. P. et al., A protein extraction method compatible with proteomic analysis for the euhalophyte *Salicornia europaea*. *Electrophoresis* 2007, **28**, 3976–3987.
- [51] Wang, N. L., Duan, X. M., Lu, Q. J., Xue, P. et al., Proteomic analysis of aqueous humor from patients with myopia. *Mol. Vis.* 2008, **14**, 370–377.
- [52] Thimm, O., Blasing, O., Gibon, Y., Nagel, A. et al., MAPMAN: a user-driven tool to display genomics data sets onto diagrams of metabolic pathways and other biological processes. *Plant J.* 2004, **37**, 914–939.
- [53] Usadel, B., Nagel, A., Thimm, O., Redestig, H. et al., Extension of the visualization tool MapMan to allow statistical analysis of arrays, display of corresponding genes, and comparison with known responses. *Plant Physiol.* 2005, **138**, 1195–1204.
- [54] Reich, M., Liefeld, T., Gould, J., Lerner, J. et al., GenePattern 2.0. *Nat. Genet.* 2006, **38**, 500–501.
- [55] Sun, X. W., Peng, L. W., Guo, J. K., Chi, W. et al., Formation of DEG5 and DEG8 complexes and their involvement in the degradation of photodamaged photosystem II reaction center D1 protein in *Arabidopsis*. *Plant Cell* 2007, **19**, 1347–1361.
- [56] Wittig, I., Braun, H. P., Schagger, H., Blue native PAGE. *Nat. Protoc.* 2006, **1**, 418–428.
- [57] Zhang, L. X., Peng, L. W., Ma, J. F., Chi, W. et al., LOW PSII ACCUMULATION1 is involved in efficient assembly of photosystem II in *Arabidopsis thaliana*. *Plant Cell* 2006, **18**, 955–969.
- [58] Rose, T. M., Henikoff, J. G., Henikoff, S., CODEHOP (Consensus-DEgenerate hybrid oligonucleotide primer) PCR primer design. *Nucleic Acids Res.* 2003, **31**, 3763–3766.
- [59] Wang, X. C., Tian, W. M., Li, Y. X., Development of an efficient protocol of RNA isolation from recalcitrant tree tissues. *Mol. Biotechnol.* 2008, **38**, 57–64.
- [60] Momonoki, Y. S., Yamamoto, K., Oguri, S., Molecular cloning of oxygen-evolving enhancer genes induced by salt treatment in a halophyte, *Salicornia europaea* L. *Plant Prod. Sci.* 2009, **12**, 193–198.
- [61] Kim, J. M., Mayfield, S. P., Protein disulfide isomerase as a regulator of chloroplast translational activation. *Science* 1997, **278**, 1954–1957.
- [62] Emanuelsson, O., Nielsen, H., Brunak, S., von Heijne, G., Predicting subcellular localization of proteins based on their N-terminal amino acid sequence. *J. Mol. Biol.* 2000, **300**, 1005–1016.
- [63] Kleffmann, T., Russenberger, D., von Zychlinski, A., Christopher, W. et al., The *Arabidopsis thaliana* chloroplast proteome reveals pathway abundance and novel protein functions. *Curr. Biol.* 2004, **14**, 354–362.
- [64] Granvogl, B., Reisinger, V., Eichacker, L. A., Mapping the proteome of thylakoid membranes by *de novo* sequencing of intermembrane peptide domains. *Proteomics* 2006, **6**, 3681–3695.
- [65] Redondo-Gomez, S., Mateos-Naranjo, E., Davy, A. J., Fernandez-Munoz, F. et al., Growth and photosynthetic responses to salinity of the salt-marsh shrub *Atriplex portulacoides*. *Ann. Bot.* 2007, **100**, 555–563.
- [66] Redondo-Gomez, S., Wharmby, C., Castillo, J. M., Mateos-Naranjo, E. et al., Growth and photosynthetic responses to salinity in an extreme halophyte, *Sarcocornia frutescens*. *Physiol. Plant.* 2006, **128**, 116–124.
- [67] Bethke, P. C., Drew, M. C., Stomatal and nonstomatal components to inhibition of photosynthesis in leaves of *Capsicum annuum* during progressive exposure to NaCl salinity. *Plant Physiol.* 1992, **99**, 219–226.
- [68] Hu, L. X., Wang, Z. L., Huang, B. R., Diffusion limitations and metabolic factors associated with inhibition and recovery of photosynthesis from drought stress in a C₃ perennial grass species. *Physiol. Plant.* 2010, **139**, 93–106.
- [69] Lovelock, C. E., Ball, M., Influence of salinity on photosynthesis of halophytes, in: Läuchli, A., Lüttge, U. (Eds.), *Salinity: Environment – Plant – Molecules*, 2002, Kluwer, Dordrecht, The Netherlands, pp. 315–339.
- [70] Kuttkat, A., Edhofer, I., Eichacker, L. A., Paulsen, H., Light-harvesting chlorophyll *a/b*-binding protein stably inserts into etioplast membranes supplemented with Zn-pheophytin *a/b*. *J. Biol. Chem.* 1997, **272**, 20451–20455.
- [71] Liu, X. D., Shen, Y. G., NaCl-induced phosphorylation of light harvesting chlorophyll *a/b* proteins in thylakoid membranes from the halotolerant green alga, *Dunaliella salina*. *FEBS Lett.* 2004, **569**, 337–340.
- [72] Ma, J. F., Peng, L. W., Guo, J. K., Lu, Q. T. et al., LPA2 is required for efficient assembly of photosystem II in *Arabidopsis thaliana*. *Plant Cell* 2007, **19**, 1980–1993.
- [73] Majeran, W., Zybailov, B., Ytterberg, A. J., Dunsmore, J. et al., Consequences of C₄ differentiation for chloroplast membrane proteomes in maize mesophyll and

- bundle sheath cells. *Mol. Cell. Proteomics* 2008, 7, 1609–1638.
- [74] Cramer, W. A., Zhang, H. M., Yan, J. S., Kurisu, G. et al., Transmembrane traffic in the cytochrome *b₆f* complex. *Annu. Rev. Biochem.* 2006, 75, 769–790.
- [75] Hanke, G. T., Endo, T., Satoh, F., Hase, T., Altered photosynthetic electron channelling into cyclic electron flow and nitrite assimilation in a mutant of ferredoxin: NADPH reductase. *Plant Cell Environ.* 2008, 31, 1017–1028.
- [76] Badger, M. R., Price, G. D., The role of carbonic anhydrase in photosynthesis. *Annu. Rev. Plant Physiol. Mol. Biol.* 1994, 45, 369–392.
- [77] Nunes-Nesi, A., Fernie, A. R., Stitt, M., Metabolic and signaling aspects underpinning the regulation of plant carbon nitrogen interactions. *Mol. Plant* 2010, 3, 973–996.
- [78] Drake, B. G., Gonzalez-Meler, M. A., Long, S. P., More efficient plants: A consequence of rising atmospheric CO₂? *Annu. Rev. Plant Physiol. Mol. Biol.* 1997, 48, 609–639.
- [79] Hoshida, H., Tanaka, Y., Hibino, T., Hayashi, Y. et al., Enhanced tolerance to salt stress in transgenic rice that overexpresses chloroplast glutamine synthetase. *Plant Mol. Biol.* 2000, 43, 103–111.
- [80] Tanaka, R., Tanaka, A., Tetrapyrrole biosynthesis in higher plants. *Annu. Rev. Plant Physiol.* 2007, 58, 321–346.
- [81] Yamazaki, H., Tasaka, M., Shikanai, T., PPR motifs of the nucleus-encoded factor, PGR3, function in the selective and distinct steps of chloroplast gene expression in Arabidopsis. *Plant J.* 2004, 38, 152–163.
- [82] Bollenbach, T. J., Sharwood, R. E., Gutierrez, R., Lerbs-Mache, S. et al., The RNA-binding proteins CSP41a and CSP41b may regulate transcription and translation of chloroplast-encoded RNAs in Arabidopsis. *Plant Mol. Biol.* 2009, 69, 541–552.
- [83] Tu, S. L., Chen, L. J., Smith, M. D., Su, Y. S. et al., Import pathways of chloroplast interior proteins and the outer-membrane protein OEP14 converge at Toc75. *Plant Cell* 2004, 16, 2078–2088.
- [84] Adam, Z., Rudella, A., van Wijk, K. J., Recent advances in the study of Clp, FtsH and other proteases located in chloroplasts. *Curr. Opin. Plant Biol.* 2006, 9, 234–240.
- [85] Schlicher, T., Soll, J., Molecular chaperones are present in the thylakoid lumen of pea chloroplasts. *FEBS Lett.* 1996, 379, 302–304.
- [86] Breiman, A., Fawcett, T. W., Ghirardi, M. L., Mattoo, A. K., Plant organelles contain distinct peptidylprolyl *cis*, *trans*-isomerases. *J. Biol. Chem.* 1992, 267, 21293–21296.
- [87] Sirpio, S., Khrouchtchova, A., Allahverdiyeva, Y., Hansson, M. et al., AtCYP38 ensures early biogenesis, correct assembly and sustenance of photosystem II. *Plant J.* 2008, 55, 639–651.
- [88] Kruger, N. J., von Schaewen, A., The oxidative pentose phosphate pathway: structure and organisation. *Curr. Opin. Plant Biol.* 2003, 6, 236–246.